

On possible release of microbe-containing particulates from a Mars lander spacecraft

Kenneth Harstad, Josette Bellan*

4800 Oak Grove Drive, M/S 125-109, Jet Propulsion Laboratory, California

Institute of Technology, Pasadena, California 91109-8099

Abstract

Due to possible planet contamination, before Earth-departure, Mars landers and/or rovers are subject to strict requirements on the maximum number of attached spores or particles that carry viable microbes. Estimates of the release rates of these particles on Mars are made considering the three mechanisms of wind shear, collision with suspended dust, and collision with saltating sand particles. The first mechanism is found to apply only to particles of size greater than 10 μm , the second mechanism has a characteristic particle adhesion half life that is so long as to be of no concern, and the third mechanism is deemed of possible importance, vitally depending on attached-particle size and detailed surface characteristics of sand and spacecraft. While not investigated in detail, dust devils are shown to be possible contributors to release of microbe-containing particles.

Key words: Mars planetary protection

1 Introduction

Mars missions using spacecraft landers and/or rovers must meet strict contamination requirements, e.g., limits on possible release of viable microbes from the spacecraft. Since it is believed that most microbes are associated with particles (Lin, 2005), release may occur by dislodgment of such a particle from a spacecraft surface. (See also the particle/microbe relation as discussed in Kempf et al., 2005.) Alternately, a particular spore may be considered as a very small particle.

Microbes on Earth have a very large size range, from as small as 20 nm up to 1 mm (American Society for Microbiology website). This entire range might not be present on spacecraft surfaces. For example, *Bacillus* spores found on spacecraft surfaces have a size of $\sim 1\mu\text{m}$ (Kempf et al., 2005, Venkateswaran et al., 2004).

According to Barengoltz, 2005, the particulate specification typically employed for spacecraft cleanliness is given by the Institute of Environmental Sciences and Technology, 2002. The feature of the size distribution specified is that for every particle size increment of $\sim 25\mu\text{m}$ over the size of $1\mu\text{m}$, the survival function, which is $[1 - (\text{cumulative probability})]$, decreases by a decade. It is

* Corresponding Author

Email address: `Josette.Bellan@jpl.nasa.gov`, Tel: (818) 354-6959, Fax: (818) 393-6682 (Josette Bellan).

then expected that the count of particles of size $\sim 25 \mu\text{m}$ or larger will be relatively small. However, even if there is a very small number of particles of $\sim 50 \mu\text{m}$ size, for example, their relevance to planetary contamination may be much greater than their count would suggest because such particles may contain more spores or microbes per particle than smaller particles.

Studies on spacecraft contamination frequently use as a representative organism the spore-forming *Bacillus subtilis* to typify the response to cleaning procedures and environmental conditions (Kempf et al., 2005, Mancinelli and Klovstad, 2000, Schuerger et al., 2003, Venkateswaran et al., 2004). This is because this particular type of organism is commonly found on spacecraft surfaces and/or in assembly facilities (Schuerger et al., 2003, Venkateswaran et al., 2004) and is hardy, with high survival rates in the harsh environments that a Mars spacecraft encounters, as simulated in experiments with judiciously assumed environments (Benardini et al., 2003, Mancinelli and Klovstad, 2000, Schuerger et al., 2003). However, the particular organism *Bacillus pumilus* is more commonly found and is also more hardy than *Bacillus subtilis* (Benardini et al., 2003, Kempf et al., 2005). Using the *Bacillus* microbes, it has been found that exposures to solar UV radiation is a key factor in the survival of exposed microbes on spacecraft, with sterilization obtained in a time interval of order 10 minutes (Mancinelli and Klovstad, 2000, Schuerger et al., 2003). Microbes that are shielded from the UV radiation can survive, for example, if they are under dust particles or under a collection of other spores; this makes plausi-

ble the assumed association of viable microbes with particles and shows that concern should be focused on shaded microbes.

To determine the probability of microbe release, several factors must be taken into account. Included factors are the distribution (count and size) of surface-attached particles, relative microbe population on the particles, adhesive forces of the particles and possible dislodgment scenarios that depend on the surface roughness, surface position, etc. The dislodgment would occur by interaction of the spacecraft with the Mars atmosphere; of particular importance are possible interactions with dust and/or sandstorms (including dust devils), which are typical features of the Mars atmosphere (Basu et al., 2004). For example, the event of March 15, 2005 (Leonard, 2005), wherein the rover Spirit solar arrays were cleaned at the Gusev site on Mars, was attributed to a dust devil; the on board camera could look down and see the vanishing wheel tracks of the rover, consistent with a heavy dust loading. Animations of Gusev-site dust devils on that day are available at Jet Propulsion Laboratory, 2005 along with more quantitative information.

Because the problem of release must consider a comprehensive, basic physical description of the circumstances, and then possible scenarios under which release may be obtained, this paper is organized as follows: First, a synopsis of information on relevant conditions and properties of the Mars atmosphere is given. Next, there is a discussion of the forces and energy of particle adhesion as characterized by the Hamaker constant which depends on both of

the materials in contact. Then, there follows a description of possible terrestrial microbe-contaminated particle dislodgment by wind shear, by dust (small Martian particles entrained in the atmosphere) storms, and finally, by sand (large Martian particle) flux due to local saltation. Last, a summary and conclusion offers highlights of the possible magnitudes of these dislodgment rates and ranks the relative importance of the three mechanisms listed above.

2 Properties of the Mars atmosphere

To analyze the interaction of a landed spacecraft with the Martian atmosphere, information is necessary regarding the Mars atmosphere adjacent to its surface (i.e. up to about 1 m above it). The Mars atmospheric gas consists mostly of CO₂ (about 95% by volume) with added small amounts of N₂, Ar and water vapor. Near the surface, the pressure varies in the approximate range 5 mb to 10 mb (Crisp, 1990, Edgett and Christensen, 1991, Murphy et al., 1995, Toon et al., 1977, Zurek et al., 1992) and the temperature range is about 160 K to 290 K (Kahn, 1995, Toon et al., 1977, Wolff and Clancy, 2003, Zurek et al., 1992). The typical wind speed is up to 10 m/s, but velocities (e.g. gusts) up to about 30 m/s exist (Greeley et al., 1980, Murphy et al., 1995, Zurek et al., 1992).

Interpreted observations (Basu et al., 2004, Greeley, 2002), show that particles on Mars are typically split into two categories: sand having diameters $\geq O(10^2$

μm), and dust which may be suspended having diameters $\leq O(10 \mu\text{m})$. The information on Martian suspended dust is desirable in the form of a normalized particle size distribution, $P(\tilde{r})$, where \tilde{r} is the characteristic particle radius, and particle total number density, n .

Essentially all measurements and models deal with dust high in the atmosphere (altitudes expressed in km units), not near the surface. Since there is almost no information about dust conditions in the vicinity of the Mars surface, it will be assumed that the $P(\tilde{r})$ and n are the same adjacent to the Mars surface as in the atmosphere. (A notable exception showing particle information on the Mars surface – but not in the atmosphere near the surface – is the information from Viking Lander sites in Table I of Christensen and Moore, 1992.) Many other publications than those listed here (Chassefière et al., 1995, Clancy et al., 1995, Korablev et al., 1993, Murphy et al., 1993, Pollack et al., 1995, Toon et al., 1977, Wolff and Clancy, 2003) were scrutinized, but only the listed references provided useful information on the dust distribution.

The prevailing consensus from the referenced papers is that the data for the dust particle size distribution can be fitted by a generalized Gamma Probability Distribution Function (Γ -PDF)

$$P(\tilde{r}) = \frac{\gamma(\alpha/\gamma)^{\frac{\alpha+1}{\gamma}}}{r_m \Gamma(\frac{\alpha+1}{\gamma})} \left(\frac{\tilde{r}}{r_m}\right)^\alpha \exp\left[-\frac{\alpha}{\gamma} \left(\frac{\tilde{r}}{r_m}\right)^\gamma\right] \quad (1)$$

where Γ is the Gamma function

$$\Gamma(x) = \int_0^{\infty} y^{x-1} e^{-y} dy \text{ for } x > 0 \quad (2)$$

and α, γ and r_m are parameters of the Γ -PDF which must be specified to define the distribution. Note that $\partial P / \partial \tilde{r} = 0$ at $\tilde{r} = r_m$ which then defines the peak of the Γ -PDF. An exception to the Γ -PDF postulate is that of Pollack et al., 1995 where a log-normal PDF was assumed instead.

The value of quantity $r_{eff} \equiv \{\{\tilde{r}^3\}\} / \{\{\tilde{r}^2\}\}$ listed in Table 1 is derived from spectrometry measurements, where $\{\{\}\}$ denotes averaging over the PDF. To obtain r_{eff} , a model of radiative transfer through the atmosphere (for Mars CO₂ and dust) is used, and along with r_{eff} a variance, ν_{eff} , is obtained. Although r_{eff} and r_m are related, from our perspective, r_{eff} is not a relevant PDF parameter, but rather r_m because it defines the distribution. In Table 1 we also list information from several publications in terms of r_m and other parameters relevant to the PDF. The information in Table 1 shows that for Mars dust typically

$$r_m \approx 0.4 \mu m, \{\{\tilde{r}\}\} \doteq 0.9 \mu m, \alpha = 2 \text{ and } \gamma = 0.5. \quad (3)$$

To calculate the drag force on such a dust particle, it is necessary to determine the regime of gas-flow around the particle. Using Mars atmosphere gas property values, the gas mean free path near the surface, l_g , may be found

using an expression for gas viscosity, μ , as

$$\mu = \rho l_g a \quad (4)$$

where $a = \sqrt{2kT/(\pi m)}$, ρ is the gas density, k is Boltzmann's constant, and m is the gas molar mass (43.4 g/mol). For CO₂ at $T = 255$ K, the value of μ is 1.3×10^{-2} cP (National Institute of Standards and Technology web site); also, the speed of sound $a_s = 1.43a$ is 250 m/s. Then, using $p = 10$ mb, one obtains $\rho = 2 \times 10^{-5}$ g/cm³, which yields $l_g = 3.7 \mu\text{m}$. Since μ is roughly proportional to the temperature, the value of l_g is in the range $2 \mu\text{m}$ to $9 \mu\text{m}$.

For a particle of size \tilde{r} , the Knudsen number is defined by $Kn \equiv l_g/\tilde{r}$. For Mars dust, $Kn \geq O(1)$, which indicates that most of the dust particles are in the transition regime of gas dynamic behavior (Hidy and Brock, 1970). That is, neither the continuum flow theory (where $Kn \leq O(10^{-2})$) nor the free molecular flow theory (where $Kn \geq O(10)$) limit applies. Spanning all regimes for small Mach numbers, where the Mach number is u/a_s with u being the particle velocity relative to a gas, the drag force on the particle may be expressed as

$$F_D = f_D(Kn) \rho u a A_p \quad (5)$$

where A_p is the particle cross section area (subscript p denotes particle characteristics) and f_D is a semi-empirical function of Kn (Clift et al., 1978)

$$f_D = \frac{6Kn[15 - 3C_1Kn + C_0C_2(2 + C_1^2)Kn^2]}{15 + 12C_1Kn + 9(1 + C_1^2)Kn^2 + 18C_2(2 + C_1^2)Kn^3} \quad (6)$$

with $C_0 = 8 + \pi\alpha_m$, $C_1 = (2 - \alpha_m)/\alpha_m$, $C_2 = 1/(2 - \alpha_m)$. Parameter α_m

is the molecular accommodation coefficient, $\alpha_m \leq 1$, having a typical value 0.9 (Hidy and Brock, 1970). Using this value for α_m gives $f_D(1) = 2.5$ and $f_D(\infty) = 3.6$; thus, for dust particles, $f_D \simeq 3$. A particle settling velocity (relative to the gas) u_{se} is found from a force balance, $F_D = m_p g$, where m_p is the particle mass and $g = 3.72 \text{ m/s}^2$ is the Mars gravitational constant. The result is the estimate

$$u_{se} = 0.5 \frac{\rho_p \tilde{r} g}{\rho a} = g \tau_R \quad (7)$$

where ρ_p is the particle density and τ_R is the characteristic relaxation time for the particle slip velocity. Since the density ratio is about 10^5 near the Mars surface, for a mean value $\{\{\tilde{r}\}\} = 1 \mu\text{m}$, one finds $\tau_R = 0.3 \text{ ms}$, giving $u_{se} = 1.0 \text{ mm/s}$. At higher altitude ρ decreases (the scale height for exponential decay is 10 km) and corresponding values of u_{se} increase. Both τ_R and u_{se} also increase proportionally to particle size. The relatively small values of u_{se} for dust is what allows the dust to remain suspended in the turbulent atmosphere. If τ_f is the time scale of the turbulent motion, then for small particles $\tau_f \gg \tau_R$ and these particles then move with the gas flow. In contrast, if $\tau_f \ll \tau_R$ particles tend to settle. The boundary that distinguishes between dust and sand is at $\tau_f \approx \tau_R$.

3 Particle adhesion

Consider the general case of an irregularly shaped particle that has adhered to a surface (subscript s), as in Fig. 1 where the systems of coordinates for the analysis are also defined. We define r as the distance between one molecule in the particle and another molecule in the surface. A commonly used intermolecular potential model is that of Lennard-Jones which features a repulsive term proportional to r^{-12} and a Van der Waals attractive term proportional to r^{-6} . Considering the longer-range attraction only, the potential between a particle molecule and surface molecule is given by

$$V(r) = -Cr^{-6} \quad (8)$$

where C is a constant. The corresponding force in the r direction is

$$F_r(r) = \partial V / \partial r = 6Cr^{-7} \quad (9)$$

which projected in the vertical y direction is

$$F_y(y) = F_r \cos \theta = 6C \frac{y + \xi}{r^8} \quad (10)$$

where $\cos \theta = (y + \xi)/r$ and $r^2 = \eta^2 + (y + \xi)^2$. If we define an infinitesimal volume $dV_s = \pi d\xi d(\eta^2)$ of the surface substrate having the surface molecular number density n_s ($n_s = \rho_s/m_s$ where ρ_s is the mass density and m_s is the molecular mass), then the force on the particle molecule from the total surface

is

$$F_p = n_s \int F_y dV_s = 3\pi C n_s \int_{y^2}^{\infty} dx \int_0^{\infty} \frac{d(\eta^2)}{(\eta^2 + x)^4} = \frac{\pi}{2} C \frac{n_s}{y^4} \quad (11)$$

where $x \equiv (y + \xi)^2$, and thus the adhesion force between the entire particle and the surface is

$$F_A = \frac{\pi}{2} C n_s n_p \int \frac{dV_p}{y^4} \quad (12)$$

where dV_p is the infinitesimal volume within the particle.

For a sphere having a circular footprint on the particle of radius r_c (Fig. 1)

$$F_A \simeq \frac{\pi}{2} C n_s n_p V_p \left(\frac{1}{r_c^4} + \frac{2r_c^2}{D_p^3 y_c^3} \right) \quad (13)$$

where $D_p/2 = y + r \cos \theta$ is half of the effective particle diameter; parameter y_c represents the minimum y of the particle, since due to a repulsive force on the small scale of the contact height there is an infinitesimal gap between the particle and the surface. Enlarging the vertical direction at $y = \xi = 0$ in Fig. 1 one would find that the particle and surface are not in actual contact because on these nm scales the repulsive part of the Lennard-Jones potential, i.e. the term r^{-12} , dominates. The repulsion between atoms when they are brought very close to each other has a physical origin related to the Pauli principle: when the electronic clouds surrounding the atoms starts to overlap, the energy of the system increases abruptly.

The first term in the right hand side of eq. 13 corresponds to the sphere outside of a cone over the contact area whose apex is at the particle center. The second term describes the contribution of the contact cone; evidently, and physically,

the overwhelming contribution to F_A is from the contact cone.

As another example, for a particle that is a rectangular parallelepiped of dimensions $H \times W_1 \times W_2$ where H is the particle height,

$$F_A = \frac{\pi}{6} C n_s n_p V_p \frac{1}{H y_c^3}. \quad (14)$$

Generalizing for a particle of contact area A_c having a contact gap y_c , which can be understood as a ‘roughness’ length, the adhesion force is

$$F_A = \frac{\pi}{6} C n_s n_p \frac{A_c}{y_c^3}, \quad (15)$$

and defining the contact pressure $p_A \equiv F_A/A_c$, then

$$p_A = \frac{\pi}{6} C n_s n_p \frac{1}{y_c^3}. \quad (16)$$

By definition, the Hamaker constant is

$$C_H \equiv \pi^2 C n_s n_p \quad (17)$$

in the limit of the molecular thermal fluctuations being null. No adhesion calculations can be made without knowledge of the Hamaker constant value. This value is highly dependent on the identity of the materials involved in the contact.

3.1 *The Hamaker constant*

In Leighton, 1959 it is shown that basic quantum mechanical arguments involving electromagnetic theory lead to

$$C \approx \frac{K_p Q_d^2}{4\pi\epsilon_0} \sim \frac{e^2 a_0^5}{4\pi\epsilon_0} \quad (18)$$

where K_p is the polarizability ($\sim a_0^3$), Q_d is the electric dipole moment ($\sim ea_0$), ϵ_0 is the permittivity of free space (dielectric constant), e is the electron charge and $a_0 = 5.3 \times 10^{-11}$ m is the Bohr radius. If one defines a characteristic electric field $E^* \equiv e/(4\pi\epsilon_0 a_0^2) = 5.14 \times 10^{11}$ V/m, then $C \sim eE^* a_0^7 = F^* a_0^7$ with $F^* = 82.4$ nN, showing a range of magnitude for these quantities.

A review of the literature on the experimentally measured value of the Hamaker constant for two surfaces in contact is given in Table 2. The range of values is noticeable, as well as the variation with the identity of the materials of each of the two surfaces.

3.2 *Treatment of surface asperities*

Asperities have been shown to have a large influence on adhesion (Cooper et al., 2001, Eichenlaub et al., 2002) because they determine the roughness of the contact surfaces; in fact, it is stated in Cooper et al., 2001 that “the substrate roughness dramatically influenced the observed and predicted adhesive interaction between the particle and the substrate”. The shape (i.e. geometry)

of an asperity has a direct influence on the surface roughness. For example, asperities can have hemispherical, cone-like or cylindrical ridge geometry; in general a combination of such shapes is possible. Both fractal and Fourier series representations have been used to describe the distribution of shapes (Eichenlaub et al., 2004), and it has been shown that the mathematical form of the distribution is material specific; for example, while fractals had been shown in the past to be appropriate for a large number of engineering surfaces, in Eichenlaub et al., 2004 it is found that they are not appropriate for semiconductors for which a Fourier series representation is the accurate model. Because the distribution is material specific and this information for Mars landers is not yet available, in the following we will be qualitatively assessing the influence of the mathematical form of the asperity-geometry distribution for an ad-hoc mathematical form that is conducive to understanding the physics of adhesion.

For all examples below it is assumed that a particle with large asperities is in contact with a surface with small asperities, which can then be considered relatively to the particle contact surface as being flat. Short mathematical calculations show that for a hemispherical asperity of radius R , F_A and the adhesive pressure for that asperity are

$$F_A = \frac{C_H R}{6y_c^2}, \quad p_A = \frac{1}{\pi r_c^2} \frac{C_H R}{6y_c^2} \quad (19)$$

whereas for a conical asperity of half-angle α_c

$$F_A = \frac{C_H \tan^2 \alpha_c}{6y_c} \quad (20)$$

and for a cylindrical ridge asperity of radius R and length L

$$F_A = \frac{C_H L \sqrt{R}}{3\pi y_c^{5/2}} \bar{F}(\varepsilon_c) \doteq 8.84 \times 10^{-2} \frac{C_H L \sqrt{R}}{y_c^{5/2}} \quad (21)$$

$$\bar{F}(\varepsilon_c) = \varepsilon_c^{5/2} \int_0^{\pi/2} \frac{(\cos \beta) d\beta}{(1 + \varepsilon_c - \cos \beta)^3} \quad (22)$$

where

$$\varepsilon_c \equiv \frac{y_c}{R} \text{ and } dA = 2LR(\cos \beta) d\beta \quad (23)$$

with dA being the elemental area of the asperity. Therefore, the mean p_A over the area of all asperities, denoted by $\{\}$, is

$$\{p_A\} = \frac{C_H}{6\pi y_c^m (h + y_c)^{3-m}} \quad (24)$$

where h is a generalized asperity height and m characterizes the mean asperity shape: $m = 1$ for a sharp cone, $m = 2$ for a hemisphere, $m = 5/2$ for a ridge and $m = 3$ for a plane, i.e. in the mean $1 \leq m \leq 3$.

For generic asperities, we define the area fraction f_a of asperities on the contact area A_c , the roughness maximum gap (which may change with the particle identity even if made of same material) $y_r = h + y_c$, the fraction $\chi \equiv y_c/y_r$ of contact gap height to the roughness maximum gap, and the contact length $\delta_r \equiv \min_{\mathcal{A}_s}(y_c)$ (typically $\approx 5\text{\AA}$) where \mathcal{A}_s denotes the ensemble of all asperities on a particle. A measure of how close one can be to the surface (depends on the particle) is $\varepsilon_r \equiv \delta_r/y_r \ll 1$. Thus $\varepsilon_r \leq \chi \leq 1$. If $P(\chi)$ is a PDF describing the

geometry of asperities on the contact surface A_c of a single particle, then

$$\langle p_A \rangle = f_a \int_{\epsilon_r}^1 \{p_A\} P(\chi) d\chi = \frac{C_H f_a}{6\pi y_r^3} \int_{\epsilon_r}^1 \chi^{-m} P(\chi) d\chi \equiv \frac{C_H f_a}{6\pi y_r^3} \langle\langle \chi^{-m} \rangle\rangle \quad (25)$$

where

$$\int_{\epsilon_r}^1 P(\chi) d\chi = 1 \quad (26)$$

represents the normalization condition and $\langle\langle \rangle\rangle$ denotes the averaging over A_c .

To understand the physics behind this relationship, we choose an ad-hoc mathematical form of the PDF depending on a single parameter, $s \geq 0$ representing the asperity length

$$P(\chi) = \frac{1+s}{1-\epsilon_r^{1+s}} \chi^s. \quad (27)$$

Then

$$\langle p_A \rangle = \frac{C_H f_a}{6\pi y_r^3} \frac{1+s}{1+s-m} \frac{1-\epsilon_r^{1+s-m}}{1-\epsilon_r^{1+s}} \quad (28)$$

which shows that as parameter s increases, the probability of χ being near ϵ_r decreases, meaning that there is a smaller fraction of longer asperities.

For $\epsilon_r \rightarrow 0$, meaning that the contact length becomes null, Table 3 gives an

estimate of $\langle\langle \chi \rangle\rangle$ and of the standard deviation σ_χ^2 . The question then arises:

Is the PDF of eq. 27 a reasonable distribution, and if so, are all values $s \geq 0$

shown in Table 3 possible? To investigate this aspect, consider the following

regimes

$$\text{if } s > m - 1, \text{ then } \langle p_A \rangle \sim y_r^{-3}; \quad (29)$$

$$\text{if } s < m - 1, \text{ then } \langle p_A \rangle \sim [y_r^{3-(m-1-s)} \delta_r^{m-1-s}]^{-1}. \quad (30)$$

Equation 29 is not deemed likely, as it shows independence on mean asperity shape, on the dependency of P on the fraction of contact gap height to roughness maximum gap and on the measure of how close the particle is to the surface; this set of parameters would also produce minimal adhesion, a situation conducive to particles being removed by cleaning and thus not present on the spacecraft upon launching. Thus, it seems that $(m - s) > 1$ and $(m - s)$ together with y_r characterize the PDF. For example, for $(m - s) = 2$, one finds $\langle p_A \rangle \sim y_r^{-2}$, which is a typical functional form found in the hemispherical asperity model literature (see discussions in Eichenlaub et al., 2004 and Göttinger and Peukert, 2003) embodying the dependency shown in eq. 19; since $s \geq 0$, then $2 \leq m \leq 3$, meaning that this type of distribution describes flatter asperities. Because $1 \leq m \leq 3$, as shown through examples above, $0 \leq s \leq 2$ because $s < m - 1$. Table 3 lists for $\epsilon_r \rightarrow 0$ the spread of the distribution for several values encompassing the interval in which s has physically meaningful values. For $s = 0$, all asperity lengths are equally possible and the distribution is symmetric with respect to 0.5. For $s = 2$, one encounters a distribution with a relatively small number of large asperities, a situation that does not appear physical. The final conclusion is that for the PDF represented by eq. 27, s must take relatively small values.

3.3 The influence of asperities on adhesion energy

Since vector force diagrams could become rather complicated (and also be somewhat arbitrary when particle geometry is variable and uncertain), particle release estimates are preferably made through the energy balance, rather than force balance. For a particular asperity with shape parameter m , the work energy per unit area in moving it from a particular gap value δ_c to infinity is

$$\widetilde{W}_A = \int_{\delta_c}^{\infty} \{p_A(y_c)\} dy_c \quad (31)$$

where p_A is given by eq. 24. Consider a fixed characteristic (e.g. maximum) height above the surface $h_0 = h + \delta_c$. Integrating eq. 31 and defining $\varepsilon \equiv \delta_c/h_0$, the asperity work function is

$$\widetilde{W}_A = \frac{C_H}{6\pi h_0^2} \frac{f_m(\varepsilon)}{(m-1)\varepsilon^{m-1}} \quad (32)$$

where $\varepsilon_r \leq \varepsilon \leq 1$, the minimum gap (repulsive limit) corresponds to $\varepsilon_r \ll 1$, and function f_m has limiting values of $f_m(0) = 1$ and $f_m(1) = (m-1)/2$. An expression for f_m is found by calculating the integral of eq. 31

$$f_m = (1-\varepsilon)^{-1} + \frac{\varepsilon(\varepsilon^{m-2} - 1)}{(m-2)(1-\varepsilon)^2} \quad (33)$$

which for $m \rightarrow 2$ becomes

$$f_2 = \frac{1 - \varepsilon - \varepsilon \ln(\varepsilon^{-1})}{(1-\varepsilon)^2}. \quad (34)$$

For a surface having an area asperity fraction f_a and gap PDF $P(\varepsilon)$, the mean work function over A_c is

$$\langle \widetilde{W}_A \rangle = \frac{C_H f_a}{6\pi(m-1)h_0^2} \int_{\epsilon_r}^1 \frac{f_m(\varepsilon)P(\varepsilon)}{\varepsilon^{m-1}} d\varepsilon. \quad (35)$$

Although $P(\varepsilon)$ cannot be uniquely specified, and thus $\langle \widetilde{W}_A \rangle$ cannot be calculated for general situations, estimates based on $P(\varepsilon) \sim \varepsilon^s$ may be made to produce qualitative results. This leads to 3 possible regimes for the integral of eq. 35, denoted by I_m , which depends on ϵ_r . (Note that realistic $P(\varepsilon)$ correspond to $s < 1$.)

1. $(m - s) > 2$ (surface relatively flat)

$$I_m \approx \frac{1 + s}{(m - s - 2)\epsilon_r^{m-s-2}} \quad (36)$$

where $(m - s - 2) \leq 1$ and is expected to be 0.5 or less.

2. $(m - s) < 2$ (sharp asperities)

$$I_m \approx \text{constant}, \quad (37)$$

which is a regime of minimal adhesion energy.

3. $(m - s) \rightarrow 2$ (intermediate logarithmic limit)

$$I_m \approx (m - 1) \ln(\epsilon_r^{-1}) \quad (38)$$

indicating a weak dependence. A typical value of $\ln(\epsilon_r^{-1})$ is 3.0 corresponding to $\delta_r = 5 \text{ \AA}$ and $h_0 = 100 \text{ \AA}$.

For the special case $s \equiv 0$, $I_{3/2} \simeq 1$, $I_2 \simeq \ln(\epsilon_r^{-1}) - 1$ and $I_{5/2} \simeq 2/\sqrt{\epsilon_r} - 3$.

Overall, eqs. 36 - 38 show that I_m depends very weakly on ϵ_r . For estimates of the Mars contamination problem, this dependency may be absorbed into the parameter f_a . The final form for the estimated particle work for adhesion is

$$\langle \widetilde{W}_A \rangle \simeq 0.2 \frac{C_H f_a}{h_0^2}. \quad (39)$$

Thus, for given C_H , the adhesion energy depends only on a characteristic roughness length h_0 and the area fraction f_a .

4 Surface-particle dislodgment

Particles may be dislodged either by wind shear, and/or by dust and/or by sand colliding with the surface on which they are attached. Subscript 1 denotes the surface, subscript 2 is for the target particle, and subscript 3 labels the incoming particle. In the following, y will be a generic vertical distance above a surface.

4.1 Dislodgment by wind shear

For a characteristic spacecraft length, \mathcal{L} , and wind velocity, u , the flow Reynolds number is $\text{Re} = \rho u \mathcal{L} / \mu$. Using $u = 10$ m/s (Greeley et al., 1980, Murphy et al., 1995, Zurek et al., 1992), $\mathcal{L} = 1$ m and the ρ and μ values of section 2, gives the value $\text{Re} \approx 1.5 \times 10^4$, which indicates that the flow is typically

in the fully developed turbulence regime (Dimotakis, 2000). Thus, a particle subject to being dislodged will experience a turbulent boundary layer. It is assumed that such a particle is fully exposed to the flow, i.e., it is not hidden by surface roughness or by accumulated surface coverage by dust. Since it is threshold conditions that are here of interest rather than a complete description of energetics, the analysis will be performed in terms of forces and moment balances.

According to Schlichting, 1955, the flow shear at the surface is given by $\tau_s = (\mu \partial u / \partial y)_{y=0} = \rho u_*^2$, which defines a characteristic friction velocity, u_* . Also, the shear may be expressed by the friction coefficient, c_f , as $\tau_s = 0.5 c_f \rho u^2$ (Schlichting, 1955). Values of c_f depend on surface roughness and flow geometry, however, a typical value is $O(10^{-2})$ (Schlichting, 1955), giving the relation $u_* \approx 0.1u$. Following Schlichting, 1955, very close to the surface, turbulent boundary layers usually have a laminar sublayer whose thickness is approximately $\delta_{lam} = 5\mu/(\rho u_*)$. Using a typical value $u_* = 1$ m/s gives $\delta_{lam} \approx 3$ mm. This means that the particle will be in the sublayer which has a linear velocity profile $u_{bl} = u'y$ where $u' \equiv \rho u_*^2 / \mu$ is the surface velocity gradient. The process of dislodgment in such a shear flow is not entirely straightforward in that the flow drag force on the particle may cause it to tip over or to slide; further movement would depend on the particular conditions of the flow and surface. Focus here will be on thresholds for tipping or initiation of sliding; any initial movement is assumed to lead to eventual dislodgment.

For tipping an attached particle of height H , using eq. 5 for the drag force leads to a force moment of

$$M_D = \frac{1}{3} f_D \rho a u' H^2 A_p. \quad (40)$$

For calculating the resisting moment, M_p , the moment arm of the particle is assumed to be $2r_c$ (see Fig. 1) resulting in

$$M_p \approx C_H f_a \left(\frac{r_c}{y_r} \right)^3 \quad (41)$$

which represents a minimal value of M_p . To obtain this minimal value, the Van der Waals adhesion in eq. 41 has been taken as being characterized by $(m - s) \approx 1$ (e.g., $\langle p_A \rangle \sim C_H f_a y_r^{-3}$, see eqs. 28 – 30).

The criterion for tipping is $M_D \geq M_p$, which leads to a lower bound value of H , $H_t \leq H$. This value is calculated for dust with $f_D \approx 3$, giving

$$H_t \approx \frac{C_H f_a}{\rho a u'} \left(\frac{\alpha_p}{y_r} \right)^3 \quad (42)$$

where $\alpha_p \equiv r_c/H$.

Using conservative values such as $u_* = 10$ m/s, $C_H = 5 \times 10^{-20}$ J (Table 2), $\alpha_p = 0.2$, and $f_a = 10^{-2}$ along with $y_r = 10$ nm (Cooper et al., 2001, Eichenlaub et al., 2004) yields the estimate $H_t \approx 10$ μ m, representing for these conservative parameters a small value for the lower bound.

For sliding, eq. 5 leads to the force expression

$$F_D = 0.5 f_D \rho a u' H A_p. \quad (43)$$

The resistance to sliding is determined by the static friction coefficient β_f involved in calculating the sliding force

$$F_{sf} \approx \frac{C_H f_a \beta_f r_c^2}{y_r^3}. \quad (44)$$

The criterion $F_D \geq F_{sf}$ leads to defining a minimum height $H_{sf} \leq H$ such that

$$H_{sf} \approx \frac{C_H f_a \beta_{sf} \alpha_p^2}{\rho a u' y_r^3} \quad (45)$$

or $H_{sf} \approx (\beta_{sf}/\alpha_p)H_t$, which considering typical values of β_{sf} and α_p , has a value similar to H_t .

Thus, the threshold size of particles that may be dislodged by wind shear is $H \geq O(10 \mu\text{m})$. That is, essentially, only particles comparable to Martian sand size are affected by wind shear, which means that as discussed in section 1, only at most a few % of the total count will be affected.

The above calculations of the threshold value are lower bounds as they do not consider the effect of gravity. The ratio of the gravity force to the adhesion force calculated using eq. 28 with the adhesion roughness parameter $m - s = 2$, is $4\pi g \rho_p y_r^2 \delta_r H / (C_H f_a)$. Calculated using the conservative values $C_H = 5 \times 10^{-20}$ J, $f_a = 10^{-2}$, $y_r/H = 0.1$, $\delta_r = 5 \text{ \AA}$, $\rho_p = 2 \text{ g/cm}^3$ and $H = 10 \mu\text{m}$, this ratio is $\simeq 1$. This indicates that the gravity force may possibly be significant for sand size particles, and thus that the above-calculated thresholds are lower bounds, as stated.

4.2 Dislodgment by dust

Consider a dust particle colliding with a surface particle, or target, that adheres to the surface with the adhesion energy (see eq. 39)

$$W_A \simeq 0.2 \frac{C_H f_a A_c}{h_0^2} \quad (46)$$

The incoming particle kinetic energy, $K_p = 0.5m_p u_p^2$, must be greater than W_A if the target particle is to be dislodged, i.e., the energy ratio, $\beta_e \equiv W_A/K_p < 1$. (This assumes that the incoming particle remains far enough from the surface so that it acquired negligible Van der Waals energy compared to its kinetic energy.) Using a characteristic target size, H_2 , then $A_c = H_2^2$ and $m_p = 4\pi\rho_p R_p^3/3$ for a dust particle of radius R_p . Rewriting,

$$\beta_e = 0.095 \frac{C_H f_a}{\rho_p R_p^3} \left(\frac{H_2}{h_0 u_p} \right)^2 = \left(\frac{R_*}{R_p} \right)^3 \quad (47)$$

where

$$R_* = 0.46 \left(\frac{C_H f_a}{\rho_p} \right)^{1/3} \left(\frac{H_2}{h_0 u_p} \right)^{2/3}. \quad (48)$$

Because $\beta_e < 1$, only dust particles of size $R_p > R_*$ are relevant. Since both the target and dust particle will be in the laminar sublayer, the latter will have $u_p \approx u_{bl} = u'H_2/2$. Assuming the typical values $C_H = 10^{-19}$ J, $u_* = 3$ m/s, $f_a = 0.1$, $\rho_p = 2$ g/cm³ and $h_0 = 10$ nm gives a value $R_* = 10$ μ m. Comparing the value R_* to r_m and $\{\{\tilde{r}\}\}$ of eq. 3, this leads to the conclusion that only the largest dust particles (tail of the distribution) are relevant to surface particle dislodgment by dust.

It may be possible that dust settling significantly enhances the dust particle number density in the laminar sublayer. Dust flux conservation gives the change in tail distribution number density, n_t , over \mathcal{L} (flow time \mathcal{L}/u) as

$$\Delta n_t/n_t \approx \mathcal{L}u_{se}/u\delta_{lam} \quad (49)$$

where u_{se} is based on the mean tail distribution size. Taking $\tilde{r} = 20 \mu\text{m}$ and $\mathcal{L} = 1 \text{ m}$, the right hand side of the eq. 49 is approximately unity, i.e., the settling does not increase n_t in the layer by a factor of more than 2 - 3.

The information on the Mars dust PDF as shown in Table 1 reflects information based mostly on the core of $P(\tilde{r})$, not on the $P(\tilde{r})$ tail. Thus, there is major uncertainty about the distribution tail. Based on the limited information in Clancy et al., 1995 and Murphy et al., 1993, then for the tail, roughly,

$$P(R_p) \approx \frac{0.25}{\{\{\tilde{r}\}\}} \exp\left(-0.8 \frac{R_p}{\{\{\tilde{r}\}\}}\right). \quad (50)$$

If the dislodgment probability is unity for $R_p \geq R_*$ (an upper bound estimate), then the dislodgment rate, ω_D (in s^{-1}) from a dust storm is

$$\omega_D = \frac{1}{2}nH_2^3u' \int_{R_*}^{\infty} P(R_p)dR_p \quad (51)$$

where the target area is H_2^2 and $u_p = 0.5H_2u'$. Using eq. 50, the estimated dislodgment rate is

$$\omega_D \approx 0.15nH_2^3u' \exp\left(-0.8 \frac{R_*}{\{\{\tilde{r}\}\}}\right) \quad (52)$$

Taking $u_* = 3 \text{ m/s}$, $R_* = 10 \{\{\tilde{r}\}\}$, $n = 1 \text{ cm}^{-3}$ and $H_2 = 1 \mu\text{m}$ gives a corre-

sponding value $\omega_D \approx 10^{-12} \text{ s}^{-1}$. This example indicates that the dislodgment of a particle in terms of its half life is 22,000 years. Thus, one should not be concerned with dislodgment by dust.

The above derivation only holds for target particles that are not very small, i.e., of size of several μm or greater. For these larger target particles, the interaction of a dust particle in the $P(\tilde{r})$ tail with the lander surface may be neglected with respect to other, more effective interactions. For very small target particles, the interaction of both incoming and attached particles with the surface must be considered. This dual interaction means that from an operational viewpoint, the large dust particles in the dust distribution tail may be considered as effectively being part of the sand-particles category, which is treated in the next section.

4.3 Dislodgment by sand

4.3.1 Interaction of a single sand particle with a target particle

We finally consider incoming sand particles much larger than a target particle adhering to a spacecraft surface; the target particle acts in effect as an asperity on the surface.

4.3.1.1 Particle deformation The elastic deformation and inelastic deformation or losses (plastic deformation, heating and delocalization of strain

from elastic wave propagation) of the interaction among sand particle, target particle and the lander surface must to be considered since this is what determines energy partition during a collision. The possible sliding of the sand particle relative to the surface due to tangential momentum is ignored because it would most likely happen only for a small incidence angle to the surface, which is a limit unlikely to occur during saltation, and thus is not considered here. Only the energy associated with the incoming normal velocity is considered.

The elastic part of the interaction is conceptualized as that of three colinear springs, each with spring constant $k_i = A_i E_i / L_i$ where E_i is the material Young's modulus, A_i an effective cross-sectional area and L_i the effective length such that

$$L_i = A_i \int_{\text{entity } i \text{ length}} \frac{dy}{A(y)} \quad (53)$$

$$A_i L_i = \int_{\text{entity } i \text{ length}} A(y) dy \quad (54)$$

and the strain volume $V_i = A_i L_i$ at the surface $i = 1$ is limited to that of the elastic wave propagation during impact. The interaction force is $F = k_i \Delta y_i$ where Δy_i is the distortion of body i , and its corresponding strain is $\varepsilon_i = \Delta y_i / L_i$. The total distortion is given by

$$\Delta y = \sum_i \Delta y_i = F \sum_i k_i^{-1} \equiv \frac{F}{k_*} \quad (55)$$

and the strains are

$$\varepsilon_i = \frac{k_* \Delta y}{k_i L_i} = \frac{k_* \Delta y}{A_i E_i}. \quad (56)$$

If u_{n3} is the sand particle normal velocity, the corresponding kinetic energy is $K_3 = 0.5m_3u_{n3}^2$. The incoming particle also attains the Van der Waals energy, W_{A3} , given by eq. 46, in which the parameters are now: $C_{H,13}$ embodying the interaction of surface 1 with particle 3 surface, $f_{a,13}$ representing the asperity area fraction of the contact area $A_{c,13}$, and $h_{0,13}$ being the roughness height in the interaction of surface 1 and particle 3 surface. The sum of kinetic and Van der Waals energies is converted into strain energy of target particle 2 and the actual asperities. The strain energy related to the target is

$$W_{st} = 0.5 \sum_i k_i (\Delta y_i)^2 = 0.5 k_* (\Delta y)^2 = 0.5 \sum_i V_i E_i \varepsilon_i^2. \quad (57)$$

For actual asperities on the sand particle 3 or on surface 1, a similar form is obtained, denoted by W_{sa} . At the moment of kinetic energy relaxation, energy conservation is

$$K_3 + W_{A3} = W_{st} + \sum_a W_{sa} \quad (58)$$

where the sum is over all actual asperities a on A_c belonging to particle 3 and surface 1.

The plastic-and-losses part of the interaction reduces the elastic strain energies of surface 1 and target particle 2 during impact. This reduction is quantified by multiplicative factors $(c_{r,i})^2$, for $i = 1$ and 2 , where $c_{r,i}$ are the coefficients of restitution (Coaplen et al., 2004, Lu and Kuo, 2003, Sahoo and Chowdhury,

2004, Zhang and Vu-Quoc, 2002), which are dependent on the impact velocity.

The reduced strain energy is

$$W_{sr} = 0.5[k_1(c_{r,1}\Delta y_1)^2 + k_2(c_{r,2}\Delta y_2)^2]. \quad (59)$$

4.3.1.2 Incoming particle rebound For the particle 3 rebound, the following statements hold:

(a) The assumption is made that sand particle 3 moves away from target particle 2 in a very short time. To assess the validity of this assumption we calculate a characteristic motion length of a sand particle in the time interval that particle 2 responds elastically during the collision, and compare this length to the distortion of particle 2.

The collision time for the sand particle of radius R_p is given by Zhang and Vu-Quoc, 2002

$$\tau_c \simeq \frac{5R_p}{(u_{n3}a_3^4)^{1/5}} \quad (60)$$

where $a_i = \sqrt{E_i/\rho_i}$ is a characteristic speed of elastic wave propagation having a typical value of 7 km/s (see Table 4). As an example, for $R_p = 25 \mu\text{m}$ and $u_{n3} = 1 \text{ m/s}$, the collision time $\tau_c \simeq 0.1 \mu\text{s}$. The elastic response time of target particle 2 is $\tau_2 = D/a_2 \approx 0.15 \text{ ns}$ for target particle diameter $D = 1 \mu\text{m}$.

Assuming a characteristic sand particle ‘rolling rate’ $\approx \tau_c^{-1}$, the corresponding movement in $\Delta t = \tau_2$ is $\Delta L_c \approx R_p\tau_2/\tau_c$, or $\Delta L_c \approx 40 \text{ nm}$ for the values used above. (Note that $\Delta L_c/D \sim u_{n3}^{1/5}$ and is nearly constant.) In general,

assumption (a) is valid if strain $\varepsilon_2 = \Delta y_2/D \ll \Delta L_c/D \approx 0.04$; this is likely for small target particles where most of the energy transfer is to the actual asperities.

(b) After the sand particle 3 rebounds, the strain energy relaxes to free target particle 2 from surface 1 and also to provide a normal ejection velocity, u_{n2} , if $W_{sr} > W_{A2}$, where W_{A2} is the target adhesion energy. Thus

$$W_{sr} = W_{A2} + 0.5m_2u_{n2}^2. \quad (61)$$

If $W_{sr} \leq W_{A2}$, the target particle remains attached.

4.3.1.3 Target particle ejection In the following, the goal is to compare an estimate of actual asperity strain to a threshold strain for target particle ejection. The idea is to inquire what is the nature of the contact that would be sufficient to produce ejection.

In eq. 58, the kinetic energy dominates, i.e. $K_3 \gg W_{A3}$, if $R_p \gg R'_*$ for R'_* calculated using from eq. 47 with H_2 replaced by $2R_p$, h_0 by $h_{0,13}$ and u_p by u_{n3} . This results in

$$R'_* = 0.4 \frac{C_{H,13} f_{a,13}}{\rho_3} \frac{1}{(h_{0,13} u_{n3})^2}. \quad (62)$$

Using $u_{n3} = 1$ m/s and $h_{13} = 10$ nm gives $R'_* \approx 0.02$ μm . Because the value of R'_* is much smaller than a typical value of R_p , generally, the W_{A3} term is negligible in eq. 58. In the further estimates, we assume that the strain energy

of the target is small relative to the strain energies of the actual asperities, i.e. $W_{st} \ll \sum_a W_{sa}$. The mean asperity strain is then found from the relation $K_3 = \sum_a W_{sa}$. If R_a is a mean asperity radius and N_a is the asperity count, then $f_{a,13}R_p^2 = N_aR_a^2$. Hence, considering that the form of eq. 57 also holds for W_{sa} , we find that approximately

$$\sum_a W_{sa} \approx \frac{\pi}{6} f_{a,13} R_p^2 R_a E_3 \langle \varepsilon_a^2 \rangle \quad (63)$$

which yields the estimate

$$\langle \varepsilon_a^2 \rangle \approx \frac{R_p}{R_a} \frac{1}{f_{a,13}} \left(\frac{u_{n3}}{a_3} \right)^2. \quad (64)$$

A typical estimate of $\varepsilon_{a,rms} = \langle \varepsilon_a^2 \rangle^{1/2}$ is obtained for $f_{a,13} = 10^{-1}$, $R_p/R_a = 10^3$ and $u_{n3} = 1$ m/s giving the value of about $\varepsilon_{a,rms} = 10^{-2}$. This estimate provides the typical asperity strain during collision.

To estimate the threshold strain for target particle ejection, we require that $W_{sr} > W_{A2}$, or $\varepsilon_2 \geq \varepsilon_*$ where from eqs. 46 and 59

$$\varepsilon_* \approx \frac{r_{c,12}}{h_{0,12}} \left(\frac{C_{H,12} f_{a,12}}{\gamma_r V_2 E_2} \right)^{0.5} \quad (65)$$

with γ_r being a restitution parameter given by

$$\gamma_r = \frac{\pi}{4} \frac{E_2}{w_v E_1} c_{r,1}^2 + \frac{3}{2} c_{r,2}^2 \quad (66)$$

where $V_1 = w_v D^3$ and subscript 12 denotes surface/target interaction. Using $C_{H,12} = 10^{-19}$ J, $f_{a,12} = \gamma_r = 0.5$, $E_2 = 10^{11}$ N/m², $D = 1$ μ m and $h_{0,12}/r_{c,12} = 0.02$, the value $\varepsilon_* \approx 10^{-4}$ is obtained.

Values of ε_* are much less than that of $\varepsilon_{a,rms}$; it may be concluded that if the sand particle collision is such that the sand particle 3 in any way contacts (e.g. even touches) target particle 2, then particle 2 is likely to be ejected.

If the target particle 2 just happens to be at a position of a short asperity length on sand particle 3, or is very small and hidden in an asperity ‘valley’ of the surface, it will remain attached because particle 3 never contacts it. Depending on the method of spacecraft surface cleaning, the particle 2 distribution on the surface could tend to that of hidden particles; the details of the attached particles distribution as well as surface roughness distribution are vital in determination of dislodgment probabilities. If particle 2 is large enough to be certainly contacted by the sand particle, it will absorb a significant amount of impact energy and it may be assumed that it will be ejected.

4.3.2 Target particle ejection from saltation sand flux

4.3.2.1 Wind-gust saltation Another important factor in estimating possible dislodgment rates is that of the amount of sand flux from local saltation (i.e. jumps covering distance measured in meters) at the Mars surface. There is considerable literature on the process of particle lifting from the surface of Mars (Basu et al., 2004, Edgett and Christensen, 1991, Greeley et al., 1980, Greeley et al., 1992, Greeley, 2002, Greeley et al., 2003, Nishimura and Hunt, 2000). This process is of interest not only in itself, but also due to the qualita-

tive similarity to the process of particle release from a spacecraft surface. For lifting by wind shear, there is a threshold friction velocity, u_{*t} , that depends on particle size. The minimum value is $u_{*t} \approx 1$ m/s at particle diameters of about $100 \mu\text{m}$ (Edgett and Christensen, 1991, Greeley et al., 1980, Greeley et al., 1992, Greeley, 2002). The u_{*t} value rapidly increases for smaller diameters, indicating that dust lifting by wind shear is highly unlikely (Greeley, 2002). This conclusion coincides with the results of section 4.1. Wind shear thus acts on sand particles producing local saltation with jumps of about 1 m distance (Edgett and Christensen, 1991, Greeley et al., 1992).

To calculate the collision rate due to a flux of sand particles hitting a lander surface, we first consider experimental and numerical simulations of the saltation process which lead to the following estimate of the horizontal sand particle flux (Nishimura and Hunt, 2000)

$$\phi_h = \frac{C}{V_p} \frac{\rho}{\rho_p} u_* \sqrt{\frac{D_p}{D_{ch}}} \exp\left(-\frac{gy}{u_*^2}\right) \quad (67)$$

where constant $C \approx 2$, D_{ch} is a characteristic sand particle diameter whose value is $250 \mu\text{m}$ (corresponds to d_s in Nishimura and Hunt, 2000) and D_p is the particle diameter. The above flux integrated over y gives an saltation ejection rate $\sim u_*^3$ (see also Basu et al., 2004). Due to overall particle conservation during saltation (horizontal and vertical particle numbers per unit time are balanced), using the fact that the horizontal velocity is $u_h = u_e \text{ctn}(\alpha_e)$ for the injection angle $\alpha_e \in [20^\circ - 40^\circ]$ (Nishimura and Hunt, 2000) where u_e is the

vertical saltation ejection velocity, the vertical lifting flux at the Mars surface, ϕ_l , is given by

$$\phi_l \approx 2 \frac{\rho}{\rho_p} \frac{u_*^3}{u_e^2 \sqrt{D_{ch} D_p^5}} \quad (68)$$

corresponding to a single exposed sand particle lifting rate, ω_e , of

$$\omega_e \approx 0.4 \frac{\rho}{\rho_p} \frac{u_*}{\sqrt{D_{ch} D_p}} \quad (69)$$

obtained by multiplying ϕ_l by $\pi D_p^2/4$ and replacing u_e by $2u_*$ (Nishimura and Hunt, 2000).

Once the particles are lifted, if there is no turbulent dispersion of saltation trajectories, the sand particles follow ballistic (parabolic) paths and the spacecraft target area over which the particles will land will have the same value as the area from which the particles originated. When turbulence is taken into account, the lifted particles will disperse, which will increase the source area corresponding to the target area while at the same time reducing the flux density; this net effect of the two competing phenomena is ignored in the collision rate estimate made here. Also ignored here is the possible effect of electric charge on the saltating particle trajectories; as shown in Zheng et al., 2003, electrostatic force values up to that of the gravity force are indicated, depending greatly on the sand size distribution.

We calculate the dislodgment rate as the product of the sand particle collision rate and the probability that the sand particle contacts (e.g. even touches) the target particle. For a small target particle, the target area (for possible

touching) is πD_p^2 . Taking into account the sand particle flux ϕ_h variation with height y and using $\rho/\rho_p = 10^{-5}$ along with a spacecraft height y_s above Mars surface, the effective collision rate is

$$\omega_{sand} = 4\omega_e \exp\left(-\frac{gy_s}{u_*^2}\right) \approx 1.6 \times 10^{-5} \frac{u_*}{\sqrt{D_s D_p}} \exp\left(-\frac{gy_s}{u_*^2}\right). \quad (70)$$

Using values $u_* = 3$ m/s, $D_p = 100$ μ m and $y_s = 0.5$ m gives $\omega_{sand} \approx 0.25$ s⁻¹. This high rate of potential sand blasting of a surface means that dislodgment is quite probable over time, depending on the gustiness conditions and the contact probability of a target particle with a sand particle.

The estimated importance of sand saltation effects qualitatively agrees with the results on particle lifting from the Mars surface where dust lifting may occur either from impact of sand particles during saltation or by action of dust devils (Basu et al., 2004, Greeley, 2002, Greeley et al., 2003).

4.3.2.2 Dust-devil saltation While a complete and accurate description of dust devils is somewhat problematic at this point (Basu et al., 2004), some approximate characteristics can be established (Balme et al., 2003, Basu et al., 2004, Fisher et al., 2005, Greeley et al., 2003). Estimates of the dust devil track production rate (1 track corresponds to 1 dust devil), N_{dd} , have been made in Balme et al., 2003 in the range 10^{-2} to 10^2 tracks/km²-yr, with the variations corresponding to different locations on the Mars surface. The significant values of N_{dd} are concentrated mostly during the northern spring and summer, with

a mean value $O(1)$ tracks/km²-yr (Balme et al., 2003, Fisher et al., 2005). The track width varies from $\simeq 5$ m to several hundred meters, with the majority being < 50 m, and a mean of about $10 - 20$ m (Balme et al., 2003, Greeley et al., 2003, Jet Propulsion Laboratory, 2005). The mean track length range is $0.5 - 2.0$ km (Balme et al., 2003, Jet Propulsion Laboratory, 2005). Dust devils display a ‘saltation skirt’ at their bottom, adjacent to the Mars surface, that contains the larger particles (Greeley et al., 2003). The Mars Pathfinder lander apparently experienced several dust devils (Greeley et al., 2003), two of which traveled at velocities of 0.5 m/s and 4 m/s, respectively (Balme et al., 2003). The Spirit Mars rover observed on March 15, 2005 a 34 m diameter dust devil travelling at 4.8 m/s and that covered a distance of 1.6 km (Jet Propulsion Laboratory, 2005).

The above information may be used to provide an approximate description of possible dust devil activity on Mars. The track area fraction, f_{dd} , generated during a time interval Δt by a track length L_{dd} and width W_{dd} is

$$f_{dd} = N_{dd}L_{dd}W_{dd}\Delta t. \quad (71)$$

An estimate of approximately average behavior of dust devils is obtained using the values $N_{dd} = 1$ tracks/km²-yr, $L_{dd} = 1$ km, $W_{dd} = 15$ m in eq. 71: $f_{dd} \simeq 10^{-3}$ for $\Delta t = 1$ month. The quantity f_{dd} may be interpreted as the mean probability that a dust devil interacts with a spacecraft at a fixed location in a time interval Δt . Depending of location, the probability may differ by as

much as two orders of magnitude from this mean. The goal is to calculate the target particle adhesion half life resulting from dust devil interaction with the spacecraft surface.

For an approximately average dust devil velocity $u_{dd} = 1$ m/s, a typical dust devil lifetime $\tau_{dd} = L_{dd}/u_{dd} = 17$ minutes, while its interaction time with a spacecraft is $\Delta t_{dd} = W_{dd}/u_{dd} = 15$ s. Assuming that a dust-devil-skirt sand particle collision rate with a target particle has a value equal to that of ω_{sand} given in 4.3.2.1, yields a representative estimate of $(15 \text{ s} \times 0.25 \text{ s}^{-1}) \simeq 4$ sand particle collisions with the target per dust devil interaction. As an example, if the geometric contact probability between sand and target particle is $P_c = 10^{-3}$, then the adhesion probability for a number of N_{int} interactions with dust devils is found from $P_{ad} = \exp(-4P_c N_{int})$ which when calculating the half life is $P_{ad} = 0.5$ leading then to $N_{int} = \ln(2)/(4 \times 10^{-3}) = 170$. For N_{dd} given in tracks/km²-yr, the target particle adhesion half life in years is roughly

$$\Delta t_{\text{target}} = \ln(2)/[(\Delta t_{dd} \times \omega_{sand}) N_{dd} L_{dd} W_{dd} P_c] = 0.7/(4 \times 1.5 \times 10^{-2} N_{dd} P_c) \simeq 12/(N_{dd} P_c). \quad (72)$$

For a relatively high $P_c = O(10^{-1})$ and the maximum $N_{dd} = 10^2$, this results in $\Delta t_{\text{target}} = O(1)$ year, that is, a microbe-containing particle will reside on the spacecraft for a period of 1 year or longer on average before being removed by a dust devil. Of course, a happenstance encounter may occur in a much shorter time than 1 year.

A quantitative comparison on the relative importance of sand saltation from wind gusts and dust devils cannot be readily obtained. Saltation from wind gusts depends on the probability of the presence of an upwind sand patch, which in general would be highly spacecraft location specific and the distribution of sand patches is unknown and may also change as a function of time; saltation from wind gusts also depends on wind gustiness. The data on dust devils is also location dependent and quite approximate, with possible variations of over two orders of magnitude from the mean value. It may be expected that a correlation exists between sand patch presence and the strength of saltation skirts in dust devils, but this correlation is unknown. At best, some extreme upper bounds on particle dislodgment rates may be estimated separately for these two processes if the contact probabilities between sand and target particle become available.

5 Summary and conclusions

Estimates have been made of three possible dislodgment mechanisms of a microbe-carrying particle which adheres to a spacecraft surface. It has been found that wind shear can affect only relatively large particles of size about $10\ \mu\text{m}$ or larger, which represent only a few % of the total count according to the specifications.

Dislodgment by impact of suspended dust particles is estimated as correspond-

ing to an adhesion half-life of $O(10^4)$ years, and is thus not important.

The rate of saltated sand-particles (sizes greater than $10\ \mu\text{m}$) collision with the spacecraft surface near the adhered particle may be large enough to give significant dislodgment rates. The saltated particles would originate from an upwind sand patch (at distances about 1 m) during high wind ($u \geq 10\ \text{m/s}$). The dislodgment rate depends to a large extent on the probability that a sand grain contacts (e.g. even touches) the adhering particle. Thus, the dislodgment rate depends vitally on the adhering particle size, and on the roughness characteristics of the sand particles and the spacecraft surface. Also of importance is the gustiness of the Mars winds.

Dust devils may act in a manner similar to that of sand saltation generated by wind gusts. The effectiveness of dust devils depends to a large extent on spacecraft location (e.g. region of high or low activity), as well as the contact probability between sand and target.

Future work should address the transport of dislodged particles away from the spacecraft under various Mars weather conditions.

Acknowledgment

This study was conducted at the Jet Propulsion Laboratory, California Institute of Technology, and was sponsored by the National Aeronautics and Space

Administration under the Mars Contamination Program. Mrs. Elly Ponce is thanked for the drawing of Figure 1. Dr. Jack Barengoltz and Dr. Jason Kastner are thanked for their careful reading of the manuscript.

References

- American Society for Microbiology website, <http://www.microbeworld.org/home.htm>
- Balme, M. R., Whelley, P. L., Greeley, R., 2003. Mars: Dust devil track survey in Argyre Planitia and Hellas Basin. *J. Geophys. Res.* 108(E8), 5086-5094.
- Barengoltz, J., 2005. private communication.
- Basu, S., Richardson, M. I., Wilson, R. J., 2004. Simulation of the Martian dust cycle with the GFDL Mars GCM. *J. Geophys. Res.*, 109, E11006.
- Benardini, J. N., Sawyer, J., Venkateswaran, K., Nicholson, W. L., 2003. Spore UV and acceleration resistance of endolithic *Bacillus pumilus* and *Bacillus subtilis* isolates obtained from Sonoran desert basalt: implications for lithopanspermia. *Astrobiology* 3(4), 709-717.
- Chassefière, E., Drossart, P., Korabiev, O., 1995. Post-Phobos model for the altitude and size distribution of dust in the low Martian atmosphere. *J. Geophys. Res.* 100(E3), 5525-5539.
- Christensen, P. R., Moore, H. J., 1992. The Mars surface layer. Chapt. 21. In: Eds. Kieffer, H. H., Jakosky, B. M., Snyder, C. W. and Mathews, M. S., Mars, Arizona University Press, Tucson.
- Clancy, R. T., Lee, S. W., Gladstone, G. R., McMillan, W. W. and Rousch, T., 1995. A new model for Mars atmospheric dust based analysis of ultraviolet through

- infrared observations from Mariner 9, Viking, and Phobos. *J. Geophys. Res.* 100(E3), 5251-5263.
- Clift, R., Grace, J. R., Weber, M. E., 1978. *Bubbles, Drops, and Particles*, Academic Press, New York.
- Coaplen, J., Stronge, W. J., Ravini, B., 2004. Work equivalent composite coefficient of restitution. *Int. J. Impact Engr.* 30, 581-591.
- Cooper, K., Gupta, A., Beaudoin, S., 2001. Simulation of adhesion of particles to surfaces. *J. Colloid and Interface Science* 234, 248-292.
- Cornelis, W. M., Gabriels, D., 2004. A simple model for the prediction of the deflation threshold shear velocity of dry loose particles. *Sedimentology* 51, 39-51.
- Crisp, D. 1990. Infrared radiative transfer in the dust-free Martian atmosphere. *J. Geophys. Res.* 95, 14577-14588.
- Dimotakis, P. E., 2000. The mixing transition in turbulent flows. *J. Fluid Mech.* 409, 69-98.
- Drummond, C. J., Georgaklis, G., Chan, D. Y. C., 1996. Fluorocarbons: Surface free energies and Van der Waals interaction. *Langmuir* 12, 2617-2621.
- Edgett, K. S., Christensen, P. R., 1991. The particle size of Martian aeolian dunes. *J. Geophys. Res.* 96, 22765-22776.
- Eichenlaub, S., Chan, C., Beaudoin, S. P., 2002. Hamaker constants in integrated circuit metallization. *J. Colloid and Interface Science* 248, 389-397.
- Eichenlaub, S., Gelb, A., Beaudoin, S., 2004. Roughness models for particle adhesion. *J. Colloid and Interface Science* 280, 289-298.
- Fisher, J. A., Richardson, M. I., Newman, C. E., Szwast, M. A., Graf, C., Basu, S., Ewald, S. P., Toigo, A. D., Wilson, R. J., 2005. A survey of Martian dust devil

- activity using Mars Global Surveyor Mars Orbiter Camera images. *J. Geophys. Res.* 110(E03004), 1-18.
- Götzinger, M., Peukert, W., 2003. Dispersive forces of particle-surface interactions: direct AFM measurements and modelling. *Powder Technology* 130, 102-109.
- Greeley, R., Leach, R., White, B., Iversen, J., Pollack, J., 1980. Threshold wind speeds for sand on Mars. Wind tunnel simulations. *Geophys. Res. Lett.* 7, 121-124.
- Greeley, R., Lancaster, N., Lee, S., Thomas, P., 1992. Martian aeolian processes, sediments and features. Chapt. 22. In: Eds. Kieffer, H. H., Jakosky, B. M., Snyder, C. W. and Mathews, M. S., Mars, Arizona University Press, Tucson.
- Greeley, R., 2002. Saltation impact as a means for raising dust on Mars. *Planetary and Space Sci.* 50, 151-155.
- Greeley, R., Balme, M. R., Iversen, J. D., Metzger, S., Mickelson, R., Phoreman, J., White, B., 2003. Martian dust devils: Laboratory simulations of particle threshold, *J. Geophys. Res.* 108, (#E5), 5041-5052.
- Helmy, A. K., 1998. The limited swelling of montmorillonite. *J. Colloid and Interface Science* 207, 128-129.
- Hidy, G. M., Brock, J. R., 1970. *The Dynamics of Aerocolloidal Systems*, Pergamon Press, New York.
- Institute of Environmental Sciences and Technology, 2002. Product cleanliness levels and contamination control program. IEST-STD-CC1246D
- Jet Propulsion Laboratory, <http://photojournal.jpl.nasa.gov/catalog/PIA07253>.
- Kahn, R., 1995. Temperature measurements of a Martian local dust storm. *J. Geophys. Res.* 100, 5265-5275.

- Kempf, M. J., Chen, F., Kern, R., Venkateswaran, K., 2005. Recurrent isolation of hydrogen peroxide-resistant spores of *Bacillus pumilus* from a spacecraft assembly facility. *Astrobiology* 5(3), 391-405.
- Klimchitskya, G. L., Mohideen, U., Mostepanenko, V. M., 2000. Casimir and van der Waals forces between two plates or a sphere (lens) above a plate made of real metals. *Physical Rev. A* 61, 062107-1 – 11.
- Korablev, O. I., Krasnopolsky, V. A., Rodin, A. V., Chassefière, E., 1993. Vertical structure of Martian dust measured by solar infrared occultations from the Phobos spacecraft, *Icarus* 102, 76-87.
- Leighton, R. B., 1959. *Principles of Mordern Physics* McGraw-Hill, New York.
- Leonard, D., 2005. Mars rover gets new lease on life. *Space.com* March 15
- Lin, Y., 2005. private communication
- Lu, C.-J., Kuo, M.-C., 2003. Coefficients of restitution based on a fractal surface model. *J. Appl. Mech.* 70, 339-345.
- Mancinelli, R. L., Klovstad, M., 2000. Martian soil and UV radiation: microbial viability assessment on spacecraft surfaces. *Planetary and Space Sci.* 48, 1093-1097.
- Murphy, J. R., Haberle, R. M., Toon, O. B., Pollack, J. B., 1993. Martian global dust storms: zonally symmetric numerical simulations including size-dependent particle transport. *J. Geophys. Res.* 98(E2), 3197-3220.
- Murphy, J. R., Pollack, J. B., Haberle, R. M., Leovy, C. B., Toon, O. B., Schaeffer, J., 1995. Three-dimensional numerical simulation of Martian global dust storms. *J. Geophys. Res.* 100, 26357-26376.
- National Institute of Standards and Technology (NIST) Chemistry WebBook

(<http://webbook.nist.gov/chemistry/>)

- Nishimura, K., Hunt, J. C. R., 2000. Saltation and incipient suspension above a flat particle bed below a turbulent boundary layer. *J. Fluid Mech.* 417, 77-102.
- Pollack, J. B., Ockert-Bell, M. E., Shepard, M. K., 1995. Viking Lander image analysis of Martian atmospheric dust. *J. Geophys. Res.* 100(E3), 5235-5250.
- Sahoo, P., Chowdhury, S. K. R., 2004. Normal impact of rough surfaces in presence of adhesion. *Tribology International* 37, 667-675.
- Schlichting, H., 1955. *Boundary Layer Theory*, McGraw-Hill, New York.
- Schuerger, A. C., Mancinelli, R. L., Kern, R. G., Rothschild, L. J., McKay, C. P., 2003. Survival of endospores of *Bacillus subtilis* on spacecraft surfaces under simulated martian environments: implications for the forward contamination of Mars. *Icarus* 165, 253-276
- Soltani, M., Ahmadi, G., 1994. On particle adhesion and removal mechanisms in turbulent flows. *J. Adhesion Sci. Technol.* 8(7), 763-785.
- Toon, O. B., Pollack, J. B., Sagan, C., 1977. Physical properties of the particles composing the Martian dust storm of 1971-1972. *Icarus.* 30, 663-696.
- Venkateswaran, K., , Chung, S., Allton, J., Kern, R., 2004. Evaluation of various cleaning methods to remove *Bacillus* spores from spacecraft hardware materials. *Astrobiology* 4(3), 377-389.
- Wolff, M. J., Clancy, R. T., 2003. Constraints on the size of Martian aerosols from Thermal Emission Spectrometer observations. *J. Geophys. Res.* 108(E9), 5097-5120.
- Zhang, X., Vu-Quoc, L. , 2002. Modeling the dependence of the coefficients of restitution on the impact velocity in elasto-plastic collisions. *Int. J. Impact Engr.*

27, 317-341.

Zheng, X. J., Huang, N., Zhou, Y-H., 2003. Laboratory measurement of electrification of wind-blown sands and simulation of its effect on sand saltation movement. *J. Geophys. Res.* 108(D10), 4322-4330.

Zurek, R. W., Barnes, J. R., Haberle, R. M., Pollack, J. B., Tillman, J. E., Leovy, C. B., 1992. Dynamics of the atmosphere of Mars. Chapt. 26. In: Eds. Kieffer, H. H., Jakosky, B. M., Snyder, C. W. and Mathews, M. S., *Mars*, Arizona University Press, Tucson.

References	Mission	Measurements	Assumptions	α	γ	r_{eff} μm	r_m μm	$\{\{\tilde{r}\}\}$ μm	n cm^{-3}
Korablev et al., 1993	Phobos	IR spectroscopy at $\lambda = 1.9$ and $3.7 \mu m$.	Mie scattering theory for the dust spheres. Eddy mixing with monodisperse settling. No particle collisions.	(2)	1	1.26	(0.5)	(0.75)	$\approx 0.2 - 1.0$ at height between 15 to 25 km
Toon et al., 1977	Mariner 9	Interferometric spectrometry (IRIS).	Used 2-stream radiative transport with spherical dust.	2	0.5	(3)	0.4	1.05	na
Murphy et al., 1993	Mariner 9 Viking Lander	Simulations, not measurements (see Fig. 4 in)	Fixed dust source strength at Mars surface, 0.1-80 μm size range in 30 bins.	(2)	(0.5)	(1.7 to 3.4)	(0.25 to 0.5)	(0.7 to 1.3)	(mass fraction of dust in the atmosphere is $\approx 10^{-4}$)
Chassefière et al., 1995	Phobos 2	IR Spectrometry, Thermal radiometry (visible and near IR)	Eddy diffusivity with gravitational settling. Fit for heights between 15 and 25 km. Fit extrapolated for height ≤ 15 km.	(1)	1	1.7	(0.4)	(0.8)	$\approx 1 - 3$; near-surface estimate
Pollack et al., 1995	Viking Lander 1 and Lander 2	Visible spectrometry ($\lambda = 0.49; 0.55; 0.67; 0.69 \mu m$). IR spectrometry ($\lambda = 0.86 \mu m$)	Mie scattering for small dust. Semi-empirical model for larger dust. Dust non-spherical.	nr	nr	(1.2 to 2.3)	(≈ 0.6)	(≈ 0.75)	na
Clancy et al., 1995	Mariner 9 Viking Phobos	IR spectrometry Visible spectrometry	Estimated temperature profiles. Mie scattering for palagonite (not montmorillonite). 2 nd model taken.	2	0.5	1.2	0.17	(0.45)	relative to small particles, $\leq 10^{-4}$ for $\tilde{r} \geq 10 \mu m$
Wolff and Clancy, 2003	Mars Orbiter	Thermal Emission Spectrometer	Dust and ice particles. $nP(\tilde{r})$ is constant with altitude. Uniform dust mixing.	(2)	(0.5 to 1)	1.5	(0.2 to 0.6)	(0.5 to 0.9)	na

Table 1
Particle properties in the atmosphere of Mars. The numbers in parentheses are estimates. ‘na’ means ‘not available’; ‘nr’ means ‘not relevant’.

References	First substance	Second substance	C_H 10^{-20} J	δ_r Å
Eichenlaub et al., 2002	Ag	Ag	38	na
Eichenlaub et al., 2002; Soltani and Ahmadi, 1994	Cu	Cu	27.3; 28.3	4
Eichenlaub et al., 2002; Cornelis and Gabriels, 2004	SiO ₂	SiO ₂	7.2; 6.5	na
Eichenlaub et al., 2002	TiN	TiN	15.7 - 18.2*	na
Eichenlaub et al., 2002	Parylene-n	Parylene-n	7 - 11*	na
Eichenlaub et al., 2002	Ag	Parylene-n	12	na
Eichenlaub et al., 2002	Ag	TiN	16.4	na
Eichenlaub et al., 2002	Cu	Parylene-n	9.8 - 11.1	na
Eichenlaub et al., 2002	SiO ₂	Parylene-n	6.8 - 6.9	na
Eichenlaub et al., 2002	SiO ₂	TiN	8.8	na
Eichenlaub et al., 2002	Cu	TiN	12.3	na
Eichenlaub et al., 2002	Cu	Ag	32.5	na
Eichenlaub et al., 2002	SiO ₂	Ag	12.9	na
Eichenlaub et al., 2002	PTFE	Ag	13.7	na
Eichenlaub et al., 2002	Cu	SiO ₂	14	na
Eichenlaub et al., 2002	Cu	PTFE	13	na
Eichenlaub et al., 2002	SiO ₂	PTFE	7.6	na
Drummond et al., 1996	Teflon AF1600	Teflon AF1600	3.92	1.8
Drummond et al., 1996	Teflon AF2400	Teflon AF2400	3.63	1.8
Drummond et al., 1996	PTFE	PTFE	5 - 6	<1.7
Cooper et al., 2001	Al ₂ O ₃ (alumina)	Cu	21.7	4
Cooper et al., 2001	Al ₂ O ₃	SiO ₂	9.7	4
Götzinger and Peukert, 2003	Al ₂ O ₃	Al ₂ O ₃	11	1.65
Soltani and Ahmadi, 1994	Si	Si	23.5	4.0
Soltani and Ahmadi, 1994	C (graphite)	C	46.9	4.0
Soltani and Ahmadi, 1994	glass	glass	8.5	4.0
Soltani and Ahmadi, 1994	steel	steel	21.2	4.0
Cornelis and Gabriels, 2004	mica	mica	10.7 - 13.5	na
Helmy, 1998	montmorillonite	montmorillonite	2.25	na
Klimchitskya et al., 2000	Al	Al	36*	~ 5
Klimchitskya et al., 2000	Au	Au	44*	~ 5

Table 2

Hamaker constant values. The star asterisk denotes an estimated/calculated value, and "na" denotes "not available". δ_r is the minimum contact length. Values are provided according to known accuracy.

s	$\langle\langle\chi\rangle\rangle$	σ_χ^2	$\sigma_\chi/\langle\langle\chi\rangle\rangle$	$\langle\langle\chi\rangle\rangle - \sigma_\chi$	$\langle\langle\chi\rangle\rangle + \sigma_\chi$
0	1/2	1/12	0.58	0.21	0.79
1/2	3/5	12/175	0.44	0.34	0.86
1	2/3	1/18	0.35	0.43	0.91
3/2	5/7	20/441	0.30	0.50	0.92
2	3/4	3/80	0.26	0.56	0.94

Table 3

Estimates of the mean and standard deviation associated with eqs. 26 and 27, and of the relative spread and the values away from the mean by one standard deviation subject to the constraint $s < m - 1$; all in the limit of ϵ_r being null.

Substance	E (N/m ²)	ρ (g/cm ³)	a (km/s)	ν
Al ₂ O ₃	3.70×10^{11}	3.97	9.65	-
Silica	1.80×10^{11}	2.3 to 3.0	7.7 to 8.8	0.27
Glass	$(7 \text{ to } 8) \times 10^{10}$	2.4	5.6	0.16 to 0.27
Steel	2.15×10^{11}	8.0	5.2	0.28
Cu	1.20×10^{11}	8.9	3.7	0.35

Table 4

Values of Young's modulus, E ; density, ρ ; elastic wave speed, a ; and Poisson's ratio, ν , for some common substances. Values are provided according to known accuracy.

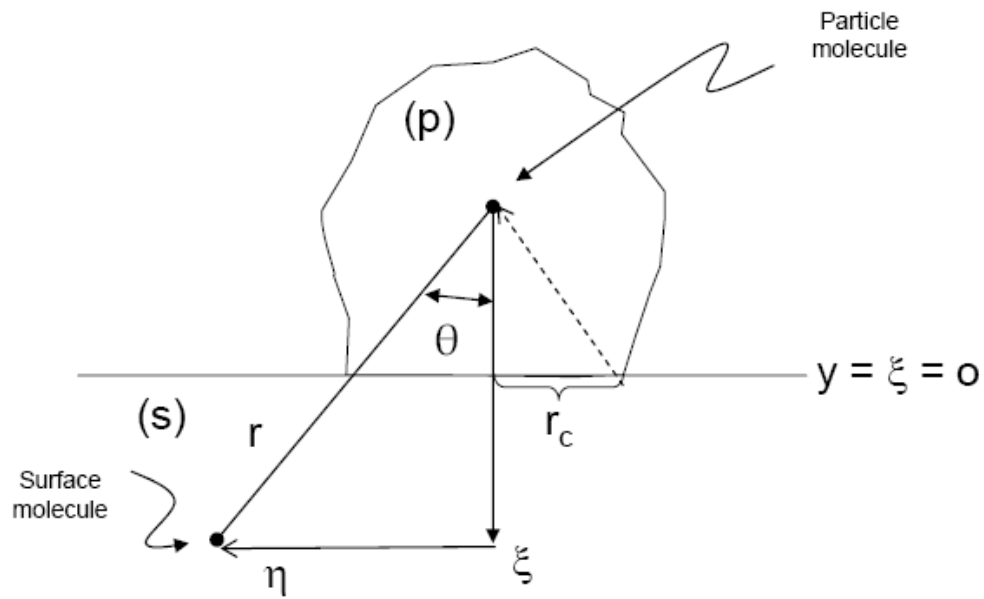


Figure 1. Configuration of a particle contact with a surface.